Role of network junctions for the totally asymmetric simple exclusion process

Adélaïde Raguin,[1,2,3,4,5] Andrea Parmeggiani,[1,2,3,4,5] and Norbert Kern[1,2]
[1]*Université Montpellier 2, Laboratoire Charles Coulomb UMR 5221, F-34095, Montpellier, France*
[2]*CNRS, Laboratoire Charles Coulomb UMR 5221, F-34095, Montpellier, France*
[3]*Université Montpellier 1, Laboratoire DIMNP UMR 5235, F-34095, Montpellier, France*
[4]*Université Montpellier 2, Laboratoire DIMNP UMR 5235, F-34095, Montpellier, France*
[5]*CNRS, Laboratoire DIMNP UMR 5235, F-34095, Montpellier, France*
(Received 3 May 2013; published 2 October 2013)

We study the effect of local regulation mechanisms on stochastic network traffic, based on simple examples. Using the totally asymmetric simple exclusion process on a multiloop structure in which several segments share a single junction, we illustrate several mechanisms: (i) additional segments improve transport but the effect saturates due to blockage, (ii) bias reduces the overall transport and leads to several regimes, (iii) "pumping" particles out of the junctions, via a locally increased hopping rate, allows us to compensate the bottlenecks but becomes futile beyond a characteristic rate which we determine. We provide a generic discussion of combinations of these effects, including phase diagrams in terms of the control parameters.

DOI: 10.1103/PhysRevE.88.042104 PACS number(s): 05.60.Cd, 87.16.Uv, 64.60.aq, 87.16.Nn

I. INTRODUCTION

Stochastic transport is a topic which is of primordial interest, both from a fundamental theoretical point of view as well as in many concrete and applied situations. The latter arise in a wide spectrum of topics, which range from the transmission of information packages over the internet, through forced diffusion of colloids, right to the motion of groups of pedestrians. The exchange of ideas between theory, experimental research, and applications has been especially fruitful for those situations where the transport takes place on one-dimensional (1D) structures or their quasi-one-dimensional extensions. This case is also particularly interesting since it is the one where the collisions between the moving objects (particles, persons, etc.) become most relevant, illustrating that the excluded volume interactions are at the heart of the collective phenomena which regulate many flow phenomena.

A paradigmatic model, which has been widely used due to both its simplicity and its versatility, has yielded much insight into such collective processes. In its simplest form, its only ingredients are the stochastic motion of particles along a 1D lattice, subject to excluded volume. This so-called totally asymmetric simple exclusion process (TASEP) was initially formulated to model protein translation [1], but it has since been transposed, adapted, and extended to represent many different systems. These include the forced motion of colloids in narrow channels [2,3], spintronics [4], the physics of molecular motors moving along the cytoskeleton [5–7], but also everyday problems such as road congestion [8], pedestrian traffic, and evacuation strategies for buildings or airplanes [9]. TASEP is well studied, both on open and closed linelike topologies, and an analytical solution is known [10–13]. Remarkably, it is also known that a simple mean-field treatment, despite its conceptual shortcomings, leads to *exact* results in many cases. This explains in part why the model has been applied so successfully, and makes it also an ideal candidate for fundamental theoretical work.

One essential aspect of many transport processes, whether they occur on the level of everyday life (roads, paths, etc.), in a more abstract medium (internet), or on a microscopic scale (colloids, molecular motors), is that the relevant underlying linelike structures are organized in a *network*. One such case which is of particular interest is intracellular transport, which is crucial to any living cell [14–17]. It can be very boldly summarized as the motion of nanometric biological machines (motor proteins), which stochastically move along a complex structure of interlinked filaments (the cytoskeleton). Although the biological complexity of these processes by far exceeds any model based on simple rules, it does appear that a generalization of TASEP captures important aspects of the collective behavior of molecular motors on biofilaments, as has been shown very recently in experiment [18].

The theoretical study of TASEP on complex networks is recent [19–22]. The quest for an analytical solution in the presence of branching remains a major challenge, even for simpler systems in equilibrium [23]. To our knowledge, no exact solution is available for TASEP on any branched structure. Nevertheless, it has been shown that significant insight can be gained into the collective processes on very complex topologies. The *junctions*, i.e., the sites where the segments of a network are interlinked, have been shown to play a crucial role since they constitute bottlenecks for the flow of particles. Blockages have been seen to arise, depending on the overall density of particles. They induce a traffic-jam-like back-lag of particles, and therefore affect the transport far beyond a local scale. Indeed, one may argue that understanding the processes at the junctions is a key to rationalizing the overall transport on the network [20,24].

Rather than tackling complex networks head on, we resort here to analyzing simple topologies in order to construct a solid understanding, which can later be transposed to large-scale complex networks. Note also that it has been demonstrated [20] that, in the absence of bias, this simple topology also directly yields a complete understanding of stationary mean-field transport on regular random networks. We combine analytical arguments with kinetic Monte Carlo simulations using random sequential update. In particular, we explore scenarios for the behavior of particles and tracks close to the junction which

affect their propensity for congestion: (i) multiple tracks, (ii) biased selection of tracks as particles leave the junction, and (iii) a locally increased activity at the junction site. We finally discuss combinations of these scenarios.

II. A BRIEF REMINDER: TOTALLY ASYMMETRIC SIMPLE EXCLUSION PROCESS ON BRANCHED TOPOLOGIES

To explore the role of junctions, we base our analysis on a simple but generic model, TASEP [1], the simple rules of which have made it a paradigm for out-of-equilibrium transport.

A. Totally asymmetric simple exclusion process

The rules defining TASEP are very simple indeed: particles move along a linear structure, taken to be a 1D lattice. They advance in a fixed direction by stochastic hops, for which the excluded volume condition requires the forward neighboring site to be empty. This is graphically summarized, for a single segment, in Fig. 1. If we wish to consider an open system, this can be achieved by imposing entrance and exit rates α and β, respectively [13].

One particularly interesting feature of TASEP is that the transport through a segment is determined by collective effects, making the behavior entirely nontrivial. For example, the current-density characteristic $J(\rho)$, which is often used to characterize the transport properties, is nonlinear due to the interactions between particles. Nevertheless, a sound understanding has been established through various techniques for TASEP on a single segment, ranging from a mean-field description, through a phenomenological description of collective effects in terms of a domain-wall (DW) theory, up to complete exact solutions of the underlying stochastic processes [10–13,25–27]. Remarkably, these analytical solutions of TASEP have shown that, despite the strong hypotheses, many mean-field results are in fact *exact* in the thermodynamic limit, making it particularly easy to exploit the model for concrete problems.

As soon as branching is introduced, however, no exact solution is known, and the effect of branching on the structure of such a solution in 1D out-of-equilibrium stochastic processes is in fact a topic of current research [23]. Nevertheless, it has been shown that it is possible to extend the mean-field analysis to branched structures, with excellent predictions when compared to kinetic Monte Carlo simulations [24,28–30]. This has recently allowed us to model the stochastic transport on large networks for TASEP [20], including additional features relevant for modeling the transport of molecular motors along the cytoskeletal network [21,22]. The approach is based on the observation that, in a mean-field spirit, the entry and exit rates α and β for an open system can be regarded as coupling the segment to an entrance reservoir of density α and an exit reservoir of density $1-\beta$ [13], and that these rates directly depend on the local connectivity [24]. This makes it possible to decompose the transport on a branched structure into single segments, for which the transport is coupled via the density on the junction sites.

Here, we shall follow this strategy in our analysis, and extend it to consider how the local properties of the junction allow us to influence the overall transport. Before proceeding further, we prepare our arguments by very briefly summarizing the main results for TASEP on a single segment.

FIG. 1. Schematic illustration of a TASEP segment with open boundary conditions. The attempt rate for a particle to enter is α, and the exit rate β. Particles hop from left to right, and interact through their excluded volume. We use $p = 1$ throughout.

B. TASEP on a single segment

For TASEP transport through a single segment, three distinct phases arise, for which the current is limited by the input rate, the output rate, or the bulk of the segment, respectively (see Fig. 1). In all phases, the density is seen to be essentially homogeneous throughout the segment, except for a small boundary zone, which occupies a negligible zone in sufficiently large segments [13]. It is set as

$$\rho = \begin{cases} \rho_{\mathrm{LD}} = \alpha & (\alpha < \beta, \alpha < 1/2), \\ \rho_{\mathrm{HD}} = 1-\beta & (\beta < \alpha, \beta < 1/2), \\ \rho_{\mathrm{MC}} = 1/2 & (\alpha, \beta > 1/2) \end{cases}$$

and the resulting phases are sketched in Fig. 2.

Owing to the homogeneous density throughout the segment, the mean-field current can be obtained in all cases from the bulk density as

$$J = \rho\,(1-\rho),$$

just as is the case for a closed ring with periodic boundary conditions.

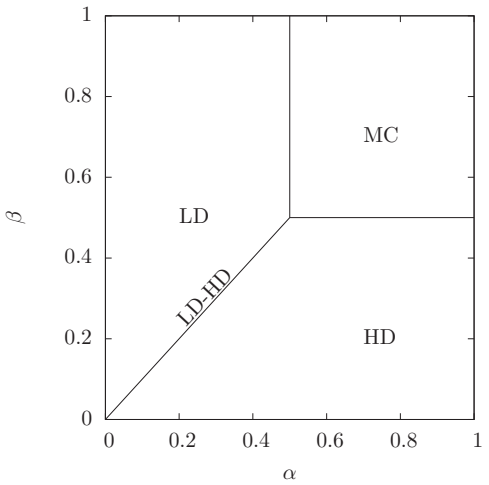

FIG. 2. Phase diagram of a single TASEP segment with open boundary conditions. According to the entry (exit) rates α (β), one of three transport regimes is established: in the LD (low density) phase the current is entry limited, in HD (high density) it is exit limited, and in MC (maximum current) it is bulk limited. LD-HD represents coexisting phases, separated by a domain wall.

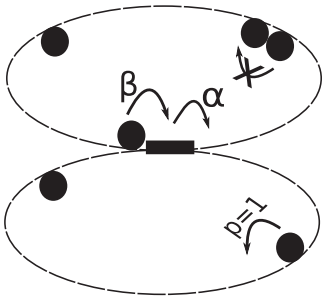

FIG. 3. Schematic illustration of TASEP on a closed-loop (figure-of-eight) topology. Particles interact through excluded volume. The effective entrance rate α and exit rate β are set through the density at the junction $\tilde{\rho}$ (see main text).

C. TASEP with a junction

The simplest topology involving a junction is the one where two TASEP rings share one site, the junction site (see Fig. 3). For this case, a mean-field analysis has shown [24] that the presence of the bottleneck caps the current through the junction at a plateau value $J = \frac{4}{9}$, for overall densities in the range $\frac{1}{3} < \rho < \frac{2}{3}$. Remarkably, for densities outside this range the junction has no effect whatsoever on the current. The current plateau is seen to correspond to a phase coexistence, in which both rings carry a downstream LD and an upstream HD section, and it can be viewed as a particle jam just upstream of where the particles enter the junction.

If a bias is introduced, such that one ring is favored over the other, then this causes the total current through the junction to drop. The current plateau is split up into two different zones, the first one corresponding to a coexistence in the favored ring, the second one in the disfavored ring. The analysis presented in our previous work is based on the following approach.

D. Effective entrance and exit rates

The main idea behind the mean-field approach of analyzing transport on the network can be summarized as treating each segment as an open TASEP system, for which the behavior is well understood. The condition of current conservation at the junction then couples the segments, and the relevant coupling parameter turns out to be the occupancy of the junction site ($\tilde{\rho}$ [24]). On a mean-field level, it amounts to setting the effective entrance and exit rates of a given segment as

$$\alpha = \frac{\tilde{\rho}_\alpha}{c_{\alpha,\mathrm{out}}} \quad \text{and} \quad \beta = 1 - \tilde{\rho}_\beta, \tag{1}$$

where $\tilde{\rho}_{\alpha,\beta}$ are the occupancies of the vertex at the entry and exit of the segment, respectively, and $c_{\alpha,\mathrm{out}}$ is the out degree of the vertex at the segment entry, i.e., the number of segments fed by this vertex. Essentially, the condition on α expresses the fact that the particles on the incoming vertex jump onto either of the (equivalent) segments it connects to; the condition on β stems from the excluded volume criterion on the junction site.

Adapting the effective rates to more general scenarios will be the key to what follows.

III. BOOSTING TRANSPORT VIA EXTRA SEGMENTS

Adding extra segments would appear to be the simplest way to improve the throughput of particles through the junction, but there is a drawback to this strategy: since adding extra segments also reinforces the bottleneck effect at the junction, it is not obvious to which extent this will increase the transport efficiency. We address the question for the simplest possible case, considering any number N of rings sharing a junction site, and we analyze the current through the junction as a function of the overall density (see Fig. 4).

The mean-field analysis can be carried out as in the case of the twofold ring. It proceeds by establishing the effective rates, identical for all segments, as

$$\alpha = \frac{\tilde{\rho}}{N} \quad \text{and} \quad \beta = 1 - \tilde{\rho}. \tag{2}$$

One then has to solve for the density $\tilde{\rho}$ on the junction site by matching the currents entering and leaving each segment. We do not present a detailed calculation here since the result may also be obtained as a special case of the more complete problem considered below, and for which Appendix A provides some detail. One finds that

$$\tilde{\rho}(\rho) = \begin{cases} N\rho & \text{if } \rho \leqslant \frac{1}{N+1} \quad \text{(LD)}, \\ \frac{N}{N+1} & \text{if } \frac{1}{N+1} < \rho < \frac{N}{N+1} \quad \text{(LD-HD)}, \\ \rho & \text{if } \rho \geqslant \frac{N}{N+1} \quad \text{(HD)}, \end{cases} \tag{3}$$

where LD-HD represents the coexistence phase giving rise to the current plateau. The corresponding *total* current $\tilde{J}$ through the junction is found to be

$$\tilde{J}(\rho) = \begin{cases} N\rho(1-\rho) & \text{if } \rho \leqslant \frac{1}{N+1} \quad \text{(LD)}, \\ \frac{N^2}{(N+1)^2} & \text{if } \frac{1}{N+1} < \rho < \frac{N}{N+1} \quad \text{(LD-HD)}, \\ N\rho(1-\rho) & \text{if } \rho \geqslant \frac{N}{N+1} \quad \text{(HD)}. \end{cases} \tag{4}$$

All rings behave identically, and we recover the behavior for the twofold ring recalled earlier for the case $N = 2$. The

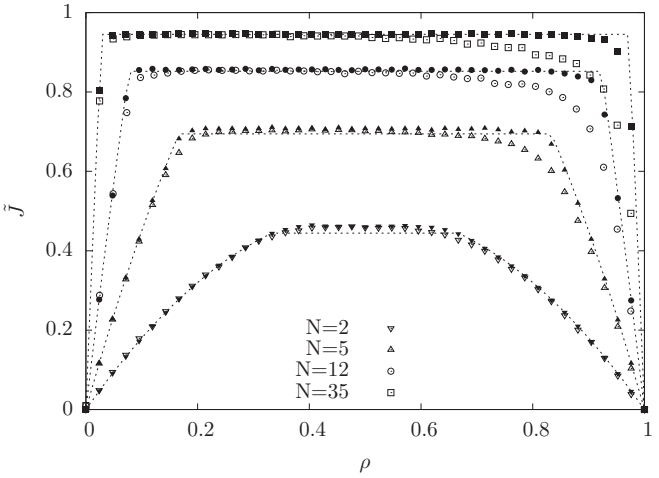

FIG. 4. Current $\tilde{J}$ through a junction shared by N loops, as a function of the overall density ρ. Lines are mean-field predictions, symbols are results from kinetic Monte Carlo simulations. We superpose data obtained with segments of length $L = 100$ (open symbols) and $L = 1000$ (full symbols) in order to illustrate how finite size effects reduce with segment size.

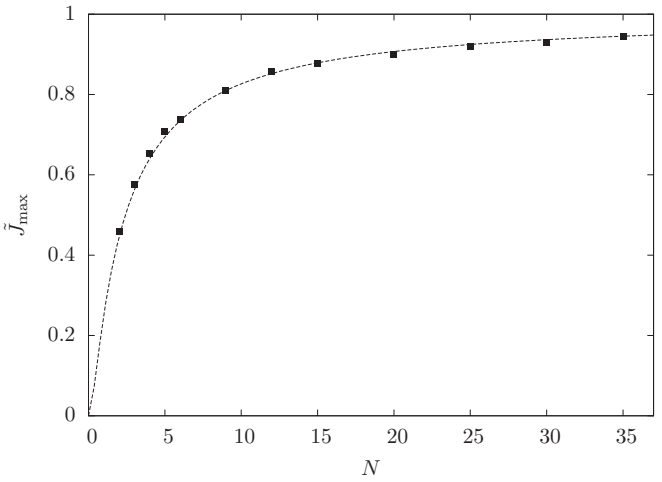

FIG. 5. Maximum (plateau) currents as a function of the number of segments sharing a junction. The saturation is due to the fact that the increased transport capacity through extra segments is progressively compensated by an increased blockage at the junction site. Data points are from simulation ($L = 100$ sites per segment), the solid line is the mean-field prediction [Eq. (4)].

current-density profiles obtained from kinetic Monte Carlo [31] simulations match these predictions extremely well (see Fig. 4). The figure also opposes simulations from a rather small ($L = 100$) system and a larger one ($L = 1000$), to illustrate that the small remaining discrepancies can be attributed to finite size effects. This validates the mean-field predictions for sufficiently large systems.

Here, we are interested in the question to which extent an increased number of segments will allow to increase the overall current. We therefore look at the *maximum* current through the junction $\tilde{J}_{\max}$, which can be achieved with N segments: this is the plateau value, as it can be read off at the center ($\rho = \frac{1}{2}$). Figure 5 confronts the mean-field predictions to results from kinetic Monte Carlo simulations, which are again in excellent agreement. It shows that this highest achievable junction current monotonously increases as the number of segments N is increased, but saturates at $\tilde{J} = 1$, as also predicted by Eq. (4).

Consequently, we can establish that there is no optimum number of segments. On the contrary, adding further segments helps the transport, but only marginally so once a significant number of segments is already present. This reflects the fact that, although additional segments do lead to an extra current, it also increases the blockage at the junction site which in turn reduces the current through any given segment. These effects ultimately balance, stabilizing the current asymptotically at $\tilde{J} = 1$ for a large number of segments sharing the junction.

IV. REGULATING MULTIPLE SEGMENTS THROUGH BIAS

In many situations we must expect to encounter a *bias*, i.e., a situation where junctions feed some of their outgoing segments more than others. This can be formalized by way of distinct rates, which may be seen as a simple way of representing complex effects, either at the junction (selection mechanism) or in the details of how the segments are connected

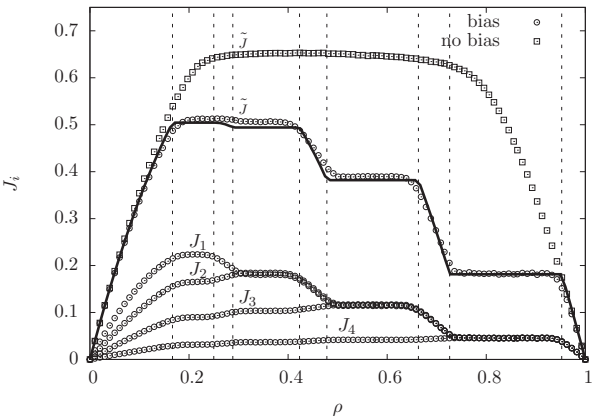

FIG. 6. Currents at the junction and in the bulk of each loop for a fourfold topology with four distinct (nondegenerate) bias parameters ($\sigma_1 = \frac{10}{20}$, $\sigma_2 = \frac{6}{20}$, $\sigma_3 = \frac{3}{20}$, $\sigma_4 = \frac{1}{20}$). The currents through individual loops progressively saturate, starting from the one with the strongest bias. At high density, the bias becomes *futile*, i.e., all loops carry the same current, *despite* the bias.

to the junction (ease with which a particular segment can be accessed, etc.). The notion of a bias, previously introduced for a twofold loop [24], has been shown to reduce the total current through the junction. This implies that the flow is optimal when both outlets are equivalent. However, rather counter-intuitively, both segments carry the same current above half-filling ($\rho > \frac{1}{2}$) whatever the bias, thereby making the bias *futile*.

We formalize the idea of a bias by attributing a parameter σ_s to each outgoing segment of a given junction. We choose to enumerate the loops in order of decreasing bias, such that

$$\sigma_1 \geqslant \sigma_2 \geqslant \cdots \geqslant \sigma_N, \quad \text{where} \quad \sum_{s=1}^{N} \sigma_s = 1. \tag{5}$$

The normalization condition accounts for the fact that all particles attempt to hop into some segment.

The full mean-field analysis again proceeds along the lines of [24] (we provide further guidance through the analysis in Appendix A). Key predictions are expressions for the currents through the segments, as well as for the total current through the junction $\tilde{J}$, as a function of the overall density ρ (see Fig. 6). The latter presents as many plateaus as there are distinct bias parameters (see Fig. 6, but also Fig. 7) for the junction occupancy. In the example, all loops have a different bias, and each plateau arises from a coexistence zone in one loop. The picture generalizes the one given previously for a biased twofold loop: as extra particles are added to the system and are redistributed according to the bias, they provoke a LD-HD coexistence first in the most favored loop. When this segment has entirely shifted to a HD phase, all others still remain in a LD phase. As further particles are added, the second loop enters coexistence until it saturates, then transits to a HD phase, and so on.

In essence, one can identify a plateau zone for each bias parameter $\sigma \in \{\sigma_1, \ldots, \sigma_N\}$, which we denote $\bar{P}^{(\sigma)} = [\rho_-^{(\sigma)}, \rho_+^{(\sigma)}]$, and which is associated with a LD-HD coexistence in the loop corresponding to the bias parameter σ. Each such plateau is then followed by a zone of decreasing current,

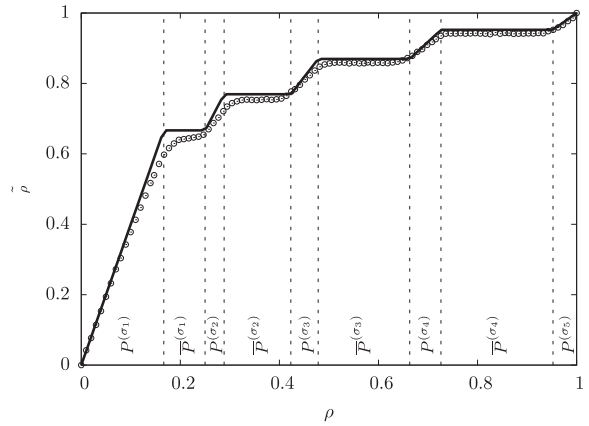

FIG. 7. Junction occupancy $\tilde{\rho}$ as a function of the overall density for a fourfold topology with four distinct (nondegenerate) bias parameters (same parameters as Fig. 6). The four successive plateaus are labeled by the associated bias parameters $\sigma \in \{\sigma_1, \ldots, \sigma_4\}$. The associated density ranges are $\bar{P}^{(\sigma)} = [\rho_-^{(\sigma)}, \rho_+^{(\sigma)}]$, whereas the subsequent range between successive plateaus are denoted as $P^{(\sigma)} = [\rho_+^{(\sigma)}, \rho_*^{(\sigma)}]$; see Appendix B [and in particular Eqs. (B3) and (B4)] for the corresponding expressions.

which we denote $P^{(\sigma)} = [\rho_+^{(\sigma)}, \rho_*^{(\sigma)}]$. ρ_* also corresponds to the beginning of the following plateau.

We refer to Appendix B for the expressions specifying these ranges since the notation is a little technical if one wishes to retain full generality, and in particular the possibility of degenerate bias parameters. Here, we restrict the discussion to highlighting the main features which follow from the expressions for the current and the associated density zones [for a full discussion, see Eq. (B10)].

First of all, as the number of segments increases, Eqs. (B7) and (B8) show that all plateaus are pushed towards lower densities: the current saturates earlier for higher connectivities. Second, for a higher number of loops, the regime of futile bias, previously known for a twofold loop, generalizes but shifts to higher densities: all individual currents are identical from the last plateau on (see Fig. 6).

V. PUMPING PARTICLES OUT OF THE JUNCTION VIA LOCALLY INCREASED HOPPING RATES

The previous considerations have provided further evidence that the role of the junctions themselves is crucial in setting the current through complex topologies, and that blockages at the junctions play a key role. Here, we explore the idea that it is the crowding of the junction site which must be tackled if we want to improve the overall flow, and we therefore introduce the notion of "pumping" particles out of the junction. By this we simply mean that particles located at a junction site are attributed a higher rate for attempting a hop. We do not intend to model any concrete physical system, but we point out that this is indeed a very natural idea: socially responsible pedestrians will adapt their behavior if told to move out of junctions as quickly as possible, traffic control through policemen (or internet routers) may be thought to have the effect of making drivers (or packages) leave junctions as quickly as possible, and one can also speculate on microscopic mechanisms for motor proteins to be more efficient in leaving a junction between filaments, for example, due to biochemical regulation or simply to the fact that more tracks to which the motors can bind are available nearby the junctions. Here, we examine the consequences of such pumping without linking the discussion to any particular system in order to highlight the potential relevance of our results for TASEP networks in general.

Here, we account for the increased activity of particles on the junction site by increasing its hopping frequency ν-fold with respect to the regular hopping rate in the bulk of the segments. In this case, the effective rate at which particles are supplied from the junction to any given segment is then given by

$$\alpha = \nu \frac{\tilde{\rho}}{N},$$

and therefore it is also increased ν-fold with respect to the regular TASEP. The exit rate, on the other hand, at which particles attempt to leave any segment to move into the junction remain unchanged ($\beta = 1 - \tilde{\rho}$) since it is only due to steric exclusion on the junction site. From this observation we can now produce mean-field predictions analytically. Following the usual procedure [24], we first determine the junction density $\tilde{\rho}$ as a function of the overall density ρ, based on the above effective rates, from which we then deduce the currents. This procedure also yields the corresponding domains for which the respective phases are present, as in a phase diagram. From this a natural distinction between two regimes arises naturally, which we discuss separately.

A. Efficient pumping ($\nu \leqslant N$)

In this first regime, we shall demonstrate that pumping indeed increases the current. To analyze the problem, we first establish the density at the junction as

$$\tilde{\rho}(\rho) = \begin{cases} \frac{N\rho}{\nu} & \text{if } \rho \in \left[0, \frac{\frac{\nu}{N}}{1+\frac{\nu}{N}}\right] \quad \text{(LD)}, \\ \frac{1}{1+\frac{\nu}{N}} & \text{if } \rho \in \left[\frac{\frac{\nu}{N}}{1+\frac{\nu}{N}}, \frac{1}{1+\frac{\nu}{N}}\right] \text{(LD-HD)}, \\ \rho & \text{if } \rho \in \left[\frac{1}{1+\frac{\nu}{N}}, 1\right] \quad \text{(HD)}, \end{cases} \tag{6}$$

which then allows us to deduce the junction current $\tilde{J}$ as a function of ρ:

$$\tilde{J}(\rho) = \begin{cases} N\,\rho(1-\rho) & \text{if } \rho \in \left[0, \frac{\frac{\nu}{N}}{1+\frac{\nu}{N}}\right] \quad \text{(LD)}, \\ \frac{\nu}{(1+\frac{\nu}{N})^2} & \text{if } \rho \in \left[\frac{\frac{\nu}{N}}{1+\frac{\nu}{N}}, \frac{1}{1+\frac{\nu}{N}}\right] \text{(LD-HD)}, \\ N\,\rho(1-\rho) & \text{if } \rho \in \left[\frac{1}{1+\frac{\nu}{N}}, 1\right] \quad \text{(HD)}. \end{cases} \tag{7}$$

In this regime, the current plateau is raised by pumping: pumping is therefore *efficient* in the plateau region, and has no effect outside the plateau. It is also clear from this result that the density region for which the LD-HD coexistence phase arises contracts progressively as ν increases. It is reduced to a point for $\nu^* = N$, which ensures coherence with the following regime of *saturated pumping*.

B. Saturated pumping ($\nu \geqslant N$)

Once the pumping rate attains the threshold $\nu^* = N$, a discontinuity arises in terms of the density at the junction

site, which is given by

$$\tilde{\rho} = \begin{cases} \frac{N\rho}{\nu} \text{ if } \rho < 1/2 \text{ (LD)}, \\ \rho \text{ if } \rho > 1/2 \text{ (HD)} \end{cases}$$
$$\text{with a density degeneracy in the MC phase} \quad (8)$$
$$\tilde{\rho} \in \left[\frac{N}{2\nu}; \frac{N}{\nu}\right] \quad \text{if } \rho = 1/2 \text{ (MC)}.$$

For the particular value of half-filling (overall density $\rho = 1/2$) mean-field predictions indicate that an infinity of densities are possible at the junction (see the vertical line in Fig. 9).

In this regime of saturated pumping, the resulting current is simply seen to saturate to that of standard TASEP

$$\tilde{J} = N\rho\,(1-\rho), \quad (9)$$

independent of the actual pumping rate. Pumping beyond the threshold ν^* thus has no further effect.

C. Discussion

The currents $\tilde{J}(\rho)$ for successively increased pumping are shown in Fig. 8, where we also compare mean-field predictions to simulation results. The agreement is very good, with some deviations at the transition regions where the system switches between phases. We can attribute these deviations to finite size effects, on the basis of the discussion accompanying similar observations in Fig. 3.

The critical threshold for the pumping rate $\nu^* = N$, revealed by the mean-field analysis, is also apparent in Fig. 8. Below this value the effect of pumping is simply to extend the density range for which the junction does not hinder the current, as is seen by the widening LD and HD zones. This happens at the expense of the intermediate density range, governed by LD-HD coexistence, for which the plateau value

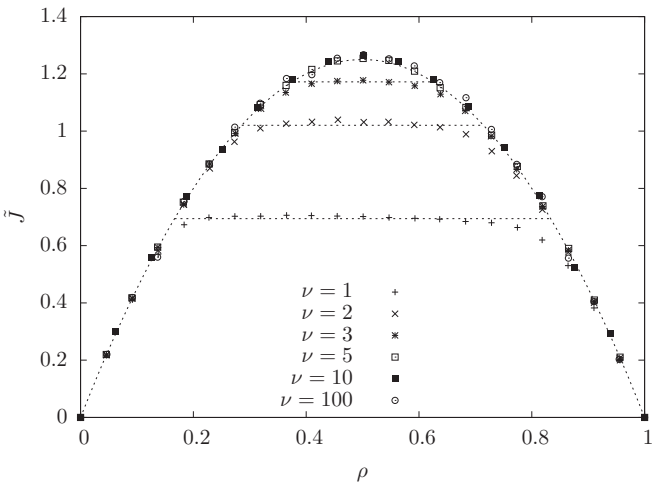

FIG. 8. Junction current $\tilde{J}$ versus overall density ρ, here for a fivefold loop ($N = 5$), for various pumping rates ν. The pumping initially raises the plateau current while reducing the relevant density zone. The underlying LD-HD phase is ultimately reduced to the single point $\rho = 1/2$, where it corresponds to a MC phase. This happens at a pumping rate $\nu^* = N$, and further pumping no longer increases the current. Deviations from predictions are attributable to finite size effects (data are for segments of length $L = 100$), as discussed before.

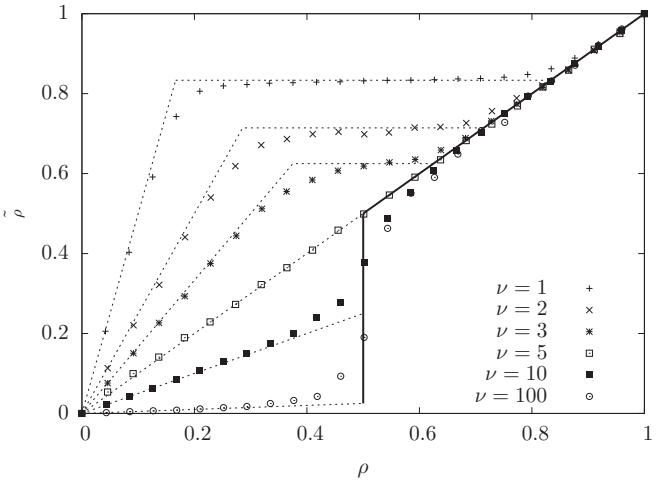

FIG. 9. Density at the junction $\tilde{\rho}$ versus overall density ρ, for a fivefold topology ($N = 5$). For the saturated pumping regime, the mean-field results do not reproduce Monte Carlo data for densities around half-filling ($\rho = 1/2$), a discrepancy which is attributed to the presence of the MC phase (see discussion in the text). In the regime of efficient pumping ($\nu \leqslant N$), the small discrepancies from mean field predictions are finite size effects.

is raised due to pumping. Recall also that the current is degenerate, in the sense that any overall density ρ in this zone leads to the same density at the junction $\tilde{\rho}$, and therefore to the same current.

The picture changes as the threshold $\nu^* = N$ is exceeded: from this point on, the current-density relation $\tilde{J}(\rho)$ is that of N independent loops, and the junction is no longer a limiting factor. This is because the current through any segment has reached its maximum value, limited by the *bulk* of the segments. Consequently, increasing the pumping at the junction can no longer increase the current any further. In this regime of *saturated pumping*, the full TASEP bulk current is recovered in all segments, implying that the junction no longer acts as a bottleneck. Increasing the pumping rate further, however, can then only depopulate the junction site and produce a boundary layer effect in the adjacent sites, as we discuss below.

A finer appreciation is provided in terms of the junction occupancy $\tilde{\rho}$ as a function of the overall density ρ, which we confront with simulations in Fig. 9. The agreement is very good for efficient pumping ($\nu \leqslant N$), and we have checked that it further improves as the segment length is increased (data not shown). This is different for the regime of saturated pumping ($\nu \geqslant N$): there it becomes apparent that what is predicted to be a discontinuous vertical jump at half-filling ($\rho = 1/2$), but appears in fact more like a crossover region of finite width. Here, the deviation from mean-field predictions is significant, and it does *not* decrease significantly for longer segments, showing that these deviations can not be attributed to simple finite size effects.

Note that this is not inconsistent with the good match for the current: the density of interest ($\rho = 1/2$) corresponds to the maximum in the current, and therefore any small deviation in density only leads to second order deviations in the current.

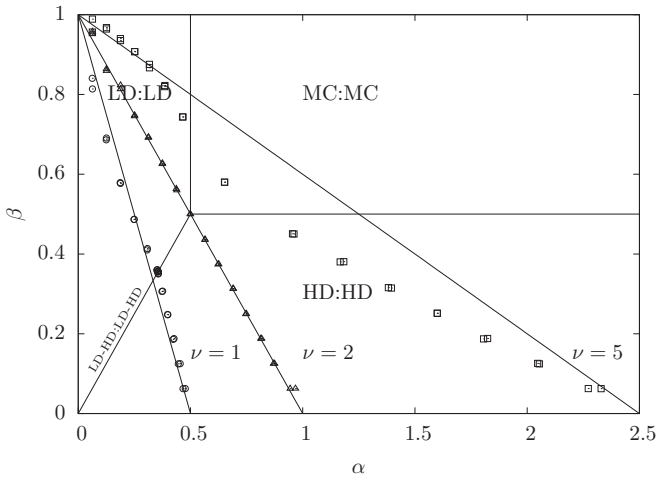

FIG. 10. Role of pumping on the effective rates, represented on the phase diagram for a twofold topology, without pumping ($\nu = 1$) and with pumping ($\nu = 5$) and with the borderline value ($\nu = 2$) for which we cross over from efficient to saturated pumping. Shown are the successive points representing the successive pairs of effective rates (α,β) as the overall density ρ is progressively increased. The slope is $-N/\nu$, and therefore decreases as the pumping rate increases. Above the threshold $\nu^* = N$, the effective rates (α,β) cross the MC zone. The notation X:Y indicates the phase in either loop, whereas X-Y stands for the coexistence of two phases on the same segment, where they are separated by a domain wall.

In order to rationalize the behavior close to half-filling, it is useful to visually contrast the regimes of efficient and saturated pumping in terms of the behavior of the individual segments. Here, we do so for a twofold loop (figure-of-eight), for simplicity and for comparison with a later scenario. Since varying the total density affects the junction occupancy $\tilde{\rho}$, this in turn changes the relevant effective rates (α,β). We therefore map out these rates, obtained from simulations run at a succession of linearly spaced overall densities. The data are shown in Fig. 10. On the ground of mean-field arguments, the points are expected to follow straight lines, which is seen directly from the definition of the effective rates ($\alpha = \nu\tilde{\rho}/N$, $\beta = 1 - \tilde{\rho}$, whence $\beta = 1 - \frac{N\alpha}{\nu}$).

First of all, these plots highlight the origin of the critical value for the pumping rate in terms of the single segment phase diagram: below $\nu^* = N$ the effective rates cross the LD-HD coexistence line, whereas above this value they evolve through the MC phase (see Fig. 10). Agreement with mean-field predictions is excellent for efficient pumping ($\nu \leqslant N$), but rather poor for saturated pumping ($\nu \geqslant N$), especially for those points close to the MC phase, but also for those in the HD region.

It is instructive to explore the reasons for these deviations. Note first of all that in the MC phase the effective rates do *not* provide a condition to fix the junction occupancy $\tilde{\rho}$ as a function of the overall density since the transport becomes boundary *independent* in this phase. Instead, all values given by Eq. (8) are compatible with the conditions for a MC phase, which is reflected in the vertical line of the mean-field prediction for $\tilde{\rho}(\rho)$ (see Fig. 9). This indeterminacy implies an additional degree of freedom susceptible to fluctuations. In particular, density fluctuations at the junction site will occur around an average value of $\rho = 1/2$, and hence their effect must be to explore both sides of the vertical transition line for $\tilde{\rho}$ ($\rho = 1/2$). This would lead to an interpolation between mean-field predictions for $\tilde{\rho}(\rho)$ on either side of the transition line $\rho = 1/2$, and this is indeed consistent with the data from simulation (see Fig. 9). In essence, this degeneracy predicted from mean-field arguments may be viewed as indicating the very points where the mean-field approach must be expected to break down as soon as fluctuations are present.

For a finer analysis, inspired by the idea of boundary layers, we turn to the occupancies of the sites next to the junction, for which we can make refined mean-field predictions (see Appendix C). Figure 11 displays the densities on the sites directly downstream and upstream from the junction site, i.e., on the first and last sites of the segments, for the case of a twofold loop.

To this end, we use refined predictions for these boundary sites, directly adjacent to the junction. They exploit the fact that the mean-field arguments given above assume constant density profiles along the segment, which is essentially true *except* for a boundary layer of a few sites at the nonlimiting boundaries. At these sites (exit in a LD segment, entry in a HD segment, both in a MC segment), a better estimate can be made by deducing the local density from the condition that the local current must match the mean-field current through the homogeneous portion of the segment. The straightforward procedure is documented in Appendix C, and the corresponding predictions are used in Fig. 11 (full lines). The main observation is that without pumping, at any overall density ρ, the exit sites have an increased occupancy as compared to the entrance sites. This indeed reflects the bottleneck effect and the back-lag of particles into the segments.

Pumping allows us to reverse this situation, as is seen in Fig. 11 (third line): for $\nu/N = 5/2$ the density at the entry sites is now *higher* than at the exit sites, at any density ρ. This points to a reversal of the bottleneck effect: the junction is no longer an obstacle, and it empties the exit sites so fast that the dynamics of the bulk can not refill it. Conversely, the entry sites are now so efficiently filled by the junction that the bulk can not absorb this surplus.

To summarize, we can conclude that the effect of actively "pumping" particles out of the junction, via an increased hopping rate on the junction site, is to raise the current plateau, up to the threshold $\nu^* = N$. Beyond this threshold, pumping fully compensates the topological handicap of sharing the junction site between several segments. Saturated pumping, beyond the value $\nu^* = N$, no longer increases the current.

VI. PUMPING VERSUS BIAS

It is now intriguing to consider a yet more complex junction which combines all previously introduced ways of modulating the transport at the junction. What is the overall flow through such a junction? Can the current drop due to the bias be compensated by pumping and, if so, to which extent and under which conditions? What phases arise? In the following, we show how to analyze this general scenario. In particular, we show that the maximum current (MC) phase plays an important role and leads to new features.

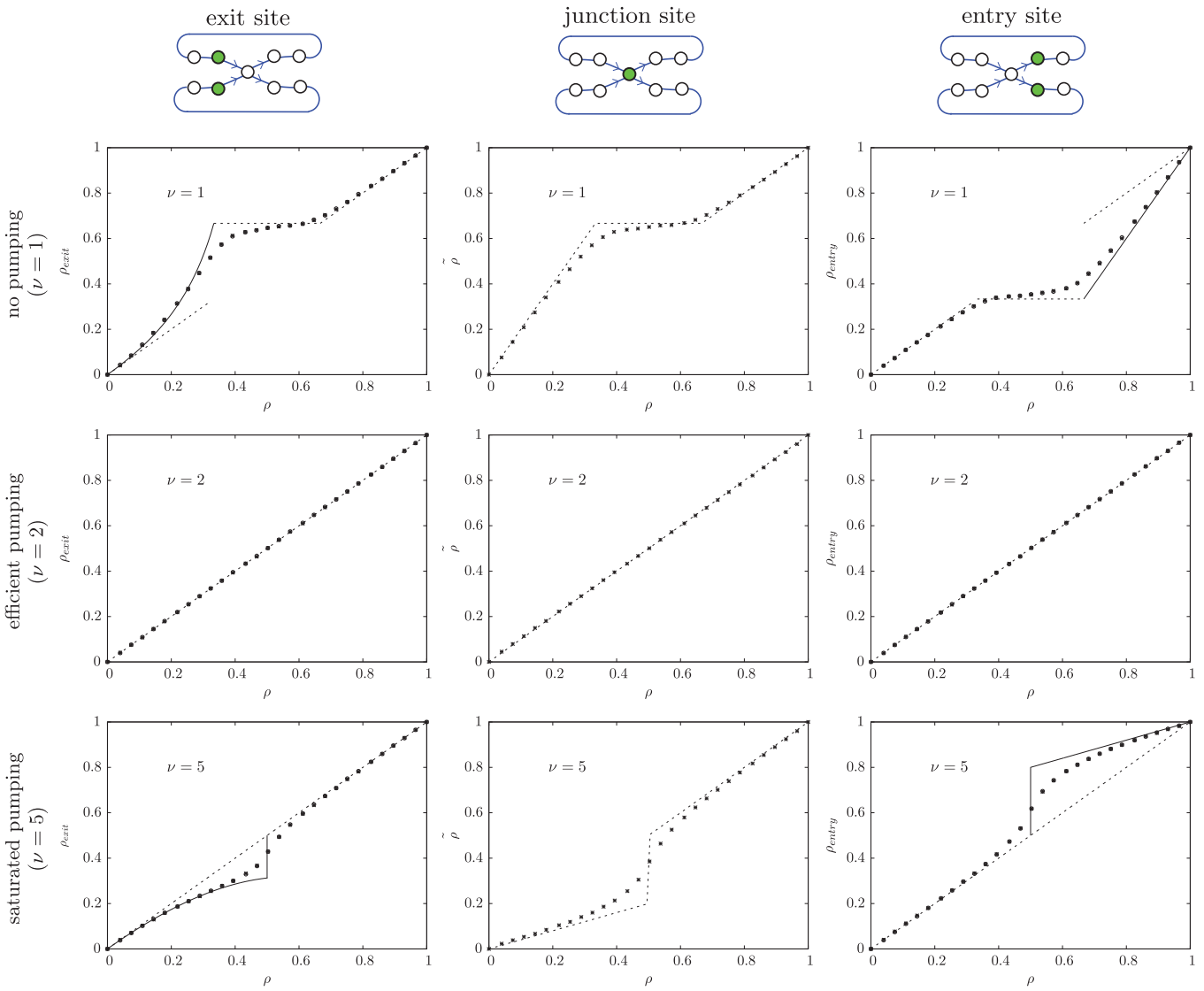

FIG. 11. (Color online) Local density at the junction and at the neighboring sites as a function of the overall density, for pumping rates $\nu = 1,2,5$ on a twofold topology. "Entry" stands for the entry site of the segments (directly fed from the junction site), whereas "exit" stands for the exit sites, i.e., the last sites in the segment, which feed the junction. Without pumping, the bottleneck effect is apparent in that the exit of segments is more likely to be occupied than the entrance sites. With $\nu = 5$ the entrance sites are fuller, whereas the exit sites (and in particular the junction) are depopulated. This is characteristic for the effect of pumping. Dashed lines are mean-field predictions; continuous lines are refined mean-field predictions taking into account boundary layer effects on the boundary sites, as discussed in the text. See Appendix D for the fully detailed expressions used to plot the graphs.

A. Pumping and bias

The question we address here is to which extent pumping particles out of the junction via an increased hopping rate can compensate the loss in transport efficiency, which is caused both by a multiple connectivity and by a bias. The approach we present is general and covers the full problem of pumping through an N-fold junction, each with an arbitrary bias; we will comment on this general case below. Full details of the calculation are provided in Appendix A for a simpler version, an N-fold loop with two distinct bias parameters. In the following, we choose to highlight the case of a twofold loop, for which we can represent the resulting phase diagrams graphically.

Note first that, in the absence of bias ($\sigma_1 = \sigma_2 = 1/2$), the critical pumping rate $\nu^* = \frac{1}{\sigma} = N$ characterizes the point where the MC phase appears, in both segments, and replaces the LD-HD coexistence at intermediate densities. When a bias is introduced there are now two critical values for pumping, as transport through either of the loops saturates:

$$\nu_1^* = \frac{1}{\sigma_1} < \frac{1}{\sigma_2} = \nu_2^*.$$

We must therefore distinguish three cases, depending on how many of the segments in LD-HD coexistence have already saturated into a MC phase: this naturally extends the notions of efficient and saturated pumping to a system with bias.

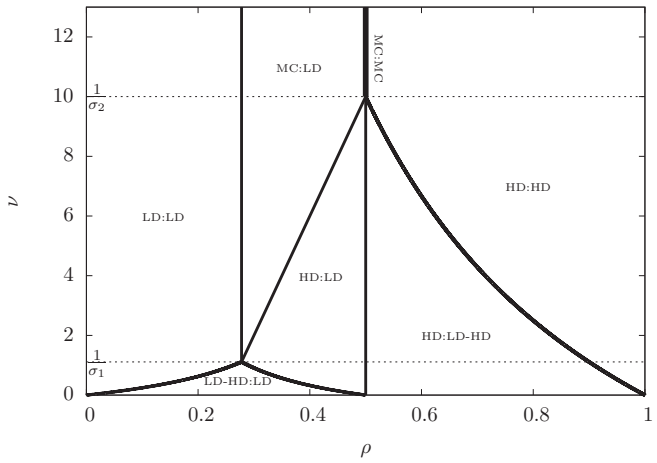

(a)Bias of 0.9 : 0.1

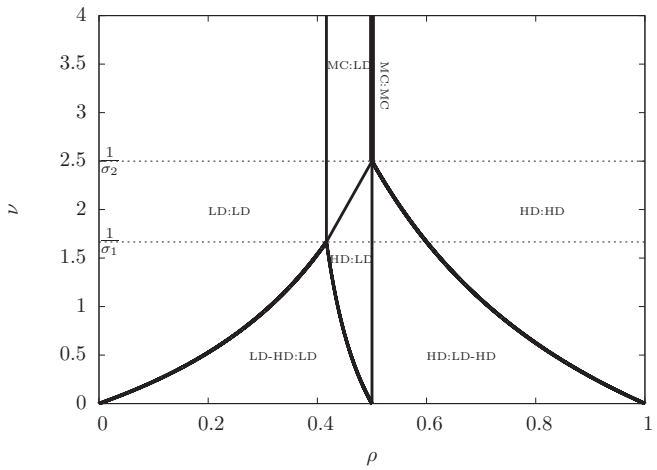

(b)Bias of 0.6: 0.4

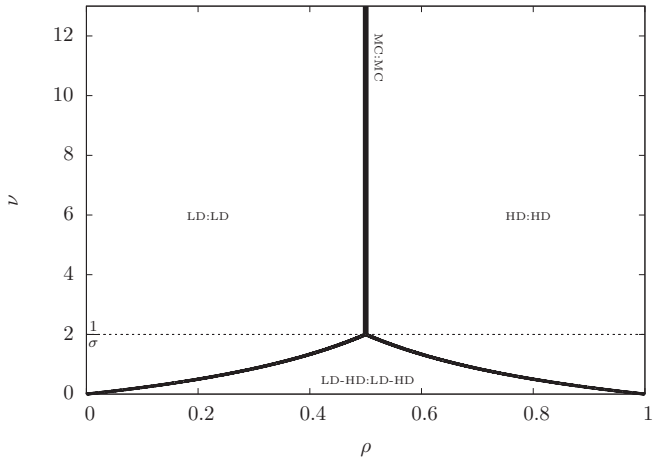

(c)No bias

FIG. 12. Complete phase diagram of a twofold loop. Phase space parameters are the pumping rate ν and the overall density ρ. Depending on the pumping rate we distinguish the regimes of (i) weak pumping ($0 < \nu < \frac{1}{\sigma_1}$), intermediate pumping ($\frac{1}{\sigma_1} < \nu < \frac{1}{\sigma_2}$), and strong pumping ($\frac{1}{\sigma_2} < \nu$). (a) Strong bias, (b) intermediate bias, (c) vanishing bias, for comparison with the above figures. Note that the scale of the ν axes differs between these figures.

For a twofold loop we have three independent parameters: one bias parameter (σ_1 and σ_2, but with $\sigma_1 + \sigma_2 = 1$), the pumping rate (ν), and the overall density (ρ). Here, we choose to fix the bias and analyze the system as a function of the other two parameters: we establish a "phase diagram" based on two parameters, the pumping rate ν and the overall density ρ (see Fig. 12).

We first present the mean-field phase diagram for a strong bias ($\sigma_1 = 0.9$, $\sigma_2 = 0.1$) in order to show the new features which arise from the simultaneous action of pumping and bias [see Fig. 12(a)]. As an example, we first focus on low values of the pumping rate. The succession of phase transitions as a function of overall density is seen to be exactly as it was in the absence of pumping: we transit from LD:LD to HD:LD to HD:HD, passing through two coexistence regions attributed to the favored then to the disfavored loop. For strong pumping, $\nu > 1/\sigma_1$, however, the favored loop is now pushed into a MC phase, whenever the overall density allows this. Therefore, there now is an extended density region for which a MC phase arises in the favored loop. As soon as this is achieved, pumping ceases to be efficient in this loop, and its current no longer increases with ν. As the pumping rate exceeds $\nu_2^* = 1/\sigma_2$, the LD-HD coexistence in the disfavored loop has been replaced entirely by a HD phase.

The topology of this phase diagram remains valid for a weaker bias [Fig. 12(b)], only the extent of the zones is modulated by the range of the corresponding pumping rates ν, as is illustrated by comparing Figs. 12(a) and 12(b); for comparison, we also show the phase diagram in the absence of bias [Fig. 12(c)].

A complementary point of view is obtained by analyzing the current at the junction as a function of the overall density (see Fig. 13) for each of the pumping regimes introduced above. The agreement between mean-field theory and simulation is very good, except for one zone which must be singled out: when at least one loop is in the regime of saturated pumping, there is a density zone for which simulations reveal a current which significantly exceeds the mean-field predictions. This zone is localized around the transition from LD:LD to MC:LD,

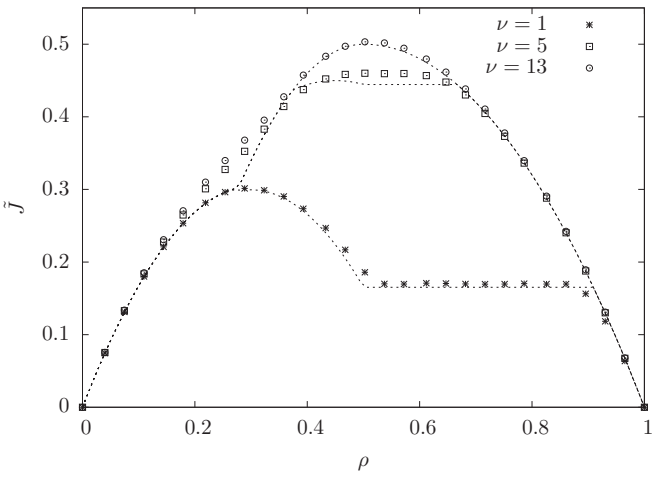

FIG. 13. Current at the junction $\tilde{J}$ versus overall density ρ in a twofold topology of $L = 100$ sites, with bias 0.9: 0.1. Several pumping rates are shown for comparison ($\nu = 1, 5, 13$).

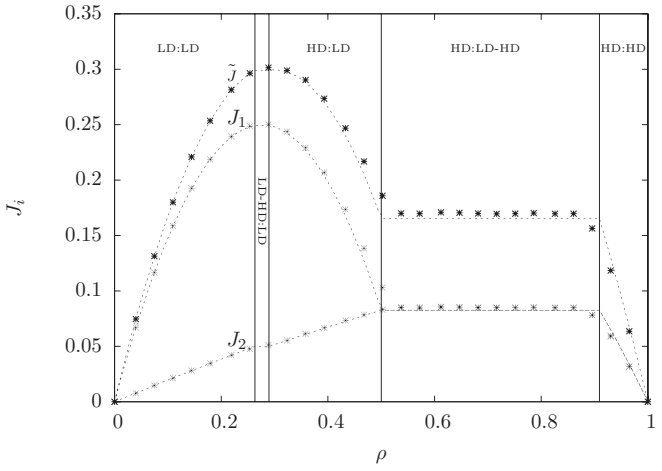

(a)$\nu = 1$: weak pumping $(\nu < \frac{1}{\sigma_1} < \frac{1}{\sigma_2})$

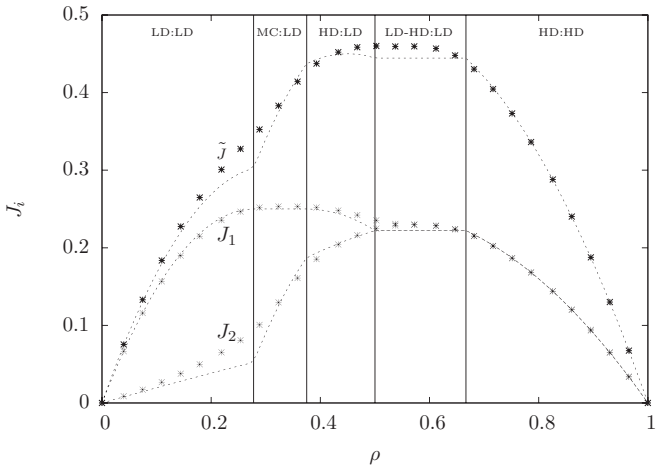

(b)$\nu = 5$: intermediate pumping $(\frac{1}{\sigma_1} < \nu < \frac{1}{\sigma_2})$

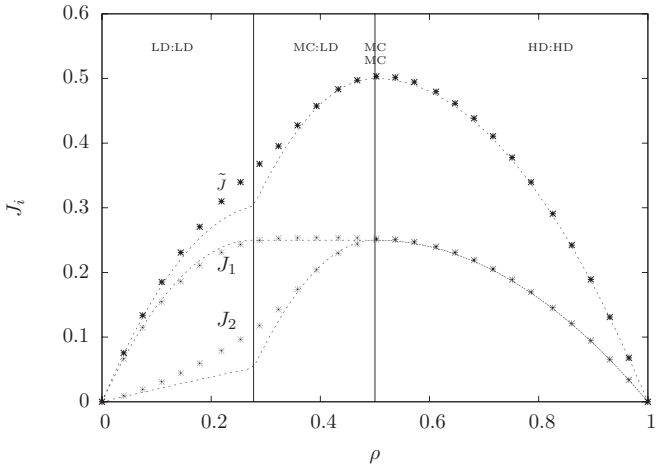

(c)$\nu = 13$: strong pumping $(\frac{1}{\sigma_1} < \frac{1}{\sigma_2} < \nu)$

FIG. 14. Currents at the junction and in the bulk of each loop versus the overall density ρ in a twofold loop of $L = 100$ sites, bias 0.9:0.1. Parameters for the graphs have been chosen to represent the respective regimes of pumping. Note that the scales are not the same for all subfigures, in order to ensure visibility. Deviations from mean-field predictions arise in the disfavored loop, but are attributed to the presence of the MC phase in the favored loop (see discussion in the text).

i.e., the density for which the favored loop switches to a MC phase [$\rho \approx \frac{1}{2N\sigma_1}$ in Fig. 14(c)].

In essence, we attribute this deviation to the presence of the MC phase, in a way similar to the case of pumping through loops without bias (Sec. V). The novelty here is that with a bias the discrepancy is also visible for the current, in contrast to the nonbiased case. To this end, the arguments employed in Sec. V suggest that any density fluctuations have different effects in both loops. In the favored section, the current carried by the MC phase is at the maximum of the parabola $J(\rho) = \rho(1-\rho)$, and therefore density fluctuations can only produce second order deviations in the current. The disfavored loop, however, is still in a LD phase, as is indeed observed in kinetic Monte Carlo simulations, and hence *not* in a current extremum. We must therefore expect density fluctuations to have a first-order effect on the current through this loop. The partial currents in each loop (Fig. 14) corroborate these interpretations: the discrepancy does indeed *not* arise in the MC segment itself, but rather in the disfavored loop.

To provide further details, we again turn to the density at the junction $\tilde{\rho}$ and at neighboring sites as a function of the overall density, which we have already seen to be a finer indicator. See Fig. 15 for the various regimes. Again, we call upon the refined mean-field arguments introduced above in order to predict the local density at the entrance and exit sites. These refined predictions are overall in good agreement with Monte Carlo simulations, but deviations arise for densities in the vicinity of the MC:LD zone, in keeping with the observations made with respect to Fig. 11. They are striking at the entry site for strong pumping, as one would expect, since pumping has a direct effect on these sites.

VII. DISCUSSION AND CONCLUSIONS

TASEP transport on branched topologies is particularly sensitive to the local dynamics at the junction sites where segments meet. This is where bottleneck effects arise and constitute a handicap for efficient transport. On the other hand, this sensitivity offers an intriguing way to regulate the overall transport by small adjustment of the local rules. We have used a topology of multiple loops sharing one junction site, in order to explore various scenarios for how the local properties affect transport: (i) adding extra segments to facilitate the flow, (ii) giving preference to certain segments via a bias, and (iii) facilitating the departure of particles from the junction site ("pumping").

As extra loops are added, the overall flow is enhanced, but only a limited improvement can be achieved. Due to saturation at the junction, any further gain by adding additional loops becomes marginal.

Biasing the particles to preferential segments allows us to boost the flow locally, but leads to a drop in the overall current. Beyond a critical density, which depends only on the number of loops, the bias becomes *futile*, in the sense that all loops carry an identical current.

An accelerated departure from the junction site by actively pumping particles out of the junction site can compensate the bottleneck effect. In the absence of bias we have identified two distinct regimes: (i) pumping is *efficient* for small pumping rates (where pumping increases the current in the coexistence

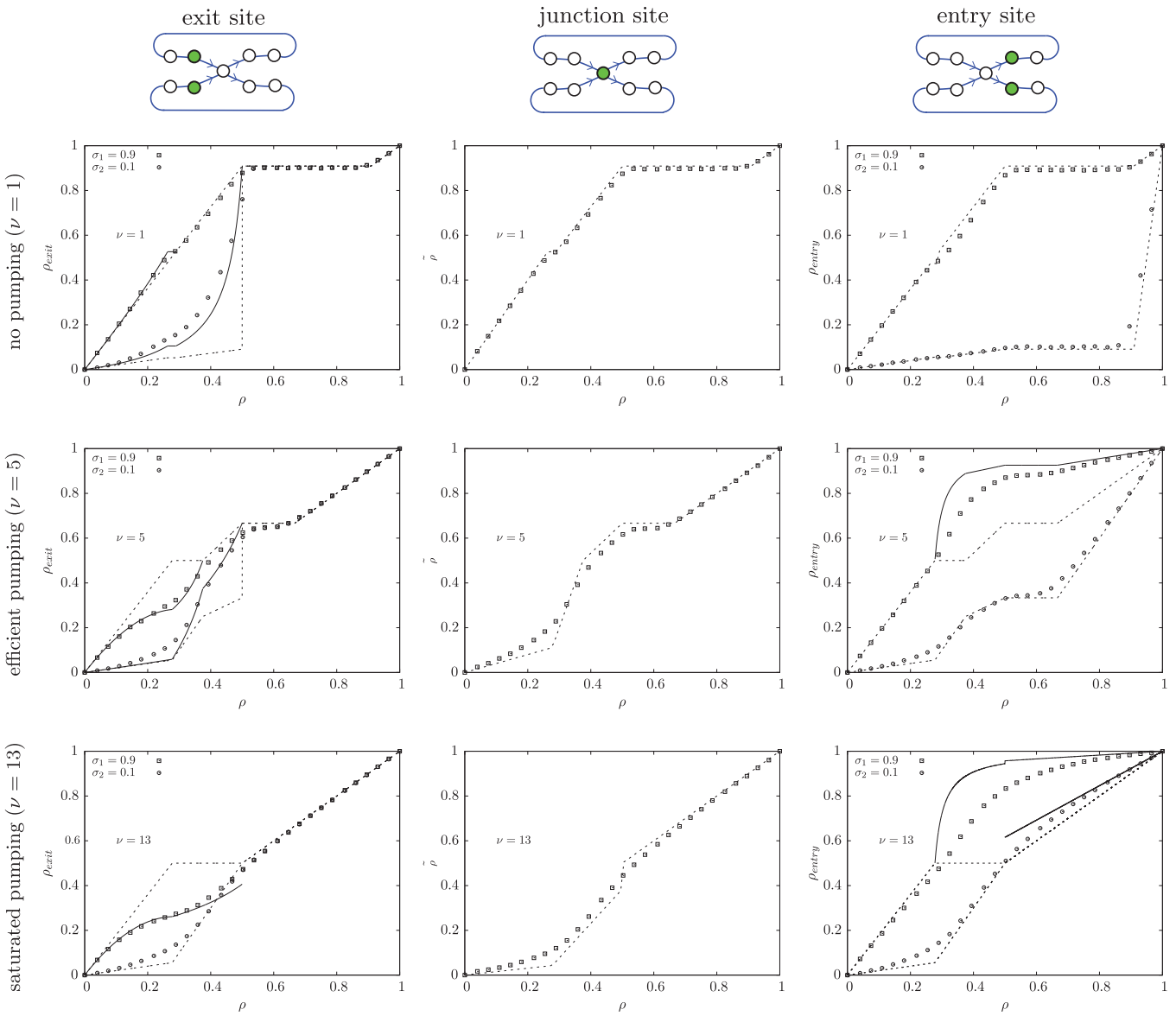

FIG. 15. (Color online) Local density at the junction and at its neighboring sites, the entry and exit sites for the segments, as a function of the overall density. We have analyzed a twofold loop with a bias of 0.9:0.1; simulations are for segments of length $L = 100$. The dashed lines indicate straightforward mean-field predictions, the continuous lines are the improved predictions from refined arguments acknowledging the particular role of the boundary sites. See Appendix D for details of mean-field predictions (some refined arguments are used again).

phase), but (ii) becomes *saturated* at a critical value set by the local vertex connectivity (where bulk dominated flow is established in all loops, such that further pumping no longer increases the current).

We have provided a generic mean-field approach for the most general case, which allows us to deduce the transport properties as a function of the overall density for any combination of these scenarios. These predictions are generally in excellent agreement with results from kinetic Monte Carlo simulations, with one restriction: when there is a bias, the favored loop may enter a MC phase. For densities close to this regime, the mean-field predictions underestimate the current, pointing to an emerging role of long-range correlations. For other cases, a refined mean-field prediction is required for the entry and exit sites of the segment, which are immediately adjacent to the junction site. This reflects the importance of boundary layers in certain regimes which, once accounted for, again lead to good predictions.

The aim of this work has been to explore various scenarios of how the overall flow can be regulated by fine-tuning the dynamics on the junctions of a network. We have therefore not intended to discuss any particular experimental situation, but there is direct potential for applying such arguments. One may, for example, think of recent experiments on molecular motors stepping along biofilaments, for which it has recently become possible to design tailor-made network structures *in vivo*, on which the motion of motors can be observed in great detail [32]. In particular, the notion of a bias arises inevitably in such a setup due to effects of steric hinderance at crosslinking points, and it is intriguing to ask how such effects will affect the

overall delivery of cargos. The network topology has already been shown to be an important feature for transport, but it emerges here that the local dynamics on the junctions provide another way to modify the flow of matter and, potentially, to regulate how material is distributed.

ACKNOWLEDGMENT

We acknowledge financial support by the CNRS and by the Scientific Council of the University Montpellier 2.

APPENDIX A: MEAN-FIELD CALCULATION

In this appendix, we reproduce the main results from mean-field arguments, following the spirit of [24]. The detailed calculations are not reproduced since they are straightforward, but we indicate the main steps.

The standard mean-field analysis is constructed from assumptions: absence of correlation between successive sites (which implies the decorrelation between distinct loops) and a homogeneous density profile along a given segment. Our calculations are based on the current conservation at the junction.

Here, we consider the case of N loops, classified in two types of n_1, n_2 loops with respective bias σ_1, σ_2, and we allow for arbitrary pumping at the junction. The approach essentially consists in envisaging all the possible combinations of phases (LD:LD, LD:HD, etc.) for the loops. For each loop, we express the effective entry (exit) rates α (β) as a function of the density at the junction $\tilde{\rho}$. This allows us to test the compatibility of phase combinations thanks to the conditions on α and β from the single-segment TASEP phase diagram. Some phase combinations are eliminated by contradictory conditions, and others are possible within certain parameter ranges.

For concreteness we provide details for one example: the LD:LD phase. The conditions can be read off directly from the phase diagram of a single TASEP segment (see Fig. 2):

$$\alpha_s < \beta_s \quad \text{and} \quad \alpha_s < \frac{1}{2} \tag{A1}$$

for all segments s. Since $\alpha_s = \nu\sigma_s\tilde{\rho}$ and $\beta_s = 1-\tilde{\rho}$ [24] we have

$$\tilde{\rho} < \frac{1}{1+\nu\sigma_s} \quad \text{and} \quad \tilde{\rho} < \frac{1}{2\nu\sigma_s} \quad \text{for all } s. \tag{A2}$$

We have also assumed $\sigma_1 > \sigma_2$ without any loss of generality, and thus two conditions hold: $\tilde{\rho} < \frac{1}{1+\nu\sigma_1}$ and $\tilde{\rho} < \frac{1}{2\nu\sigma_1}$. As a result,

$$\begin{aligned} &\text{if} \quad \nu > \tfrac{1}{\sigma_1} \Rightarrow \tilde{\rho} < \tfrac{1}{2\nu\sigma_1}, \\ &\text{if} \quad \nu < \tfrac{1}{\sigma_1} \Rightarrow \tilde{\rho} < \tfrac{1}{1+\nu\sigma_1}. \end{aligned} \tag{A3}$$

Then, the overall density ρ is just the average over the densities in each loop, which depend on the density at the junction $\tilde{\rho}$. From this we obtain $\tilde{\rho}(\rho)$. We find

$$\rho = \frac{1}{N}\sum_{s=1}^{2} n_s\rho_s \tag{A4}$$

with $\rho_s = \nu\sigma_s\tilde{\rho}$ and $\sum_{s=1}^{2} n_s\sigma_s = 1$, and thus

$$\tilde{\rho} = \tfrac{N}{\nu}\rho\ . \tag{A5}$$

The current $\tilde{J}$ at the junction is the sum of all currents through the loops, each given by $J_s = \rho_s(1-\rho_s)$. Knowing that each bulk density ρ_s is fixed either by the entrance or the exit rates, depending whether the loop is in a LD or a HD phase, we find the current as

$$\tilde{J} = \sum_{s=1}^{2} n_s J_s. \tag{A6}$$

Consequently,

$$\tilde{J} = N\rho - (N\rho)^2 \sum_{s=1}^{2} n_s\sigma_s^2. \tag{A7}$$

APPENDIX B: MULTIPLE BIAS: GENERAL CASE

The role of a bias has been illustrated and discussed in Sec. IV. Here, we provide the full mean-field solution for a junction shared by N loops, to each of which we attribute an individual bias parameter σ_s.

In the main text, we have introduced the idea that the presence of a bias leads to a succession of transitions in the loops, according to their bias: the most favored loop enters LD-HD coexistence (with a current plateau) before switching into a HD phase (with decreasing current), then the next most likely loop, and so on. This simple statement requires a little thought in terms of providing a notation for the general expressions, which must also cover the possibility of degenerate bias (several loops being equally likely). This can be achieved by distinguishing those segments which have already established a HD phase from those still in a LD phase.

The criterion for a loop (or several loops) carrying a given bias parameter $\sigma \in \{\sigma_1, \ldots, \sigma_N\}$ to display coexistence is given by

$$\alpha^{(\sigma)} = \beta^{(\sigma)}, \qquad \text{i.e.,} \qquad \sigma\,\tilde{\rho}^{(\sigma)} = 1-\tilde{\rho}^{(\sigma)}, \tag{B1}$$

which translates to

$$\tilde{\rho}^{(\sigma)} = \frac{1}{1+\sigma} \qquad (\rho \in \bar{P}^{(\sigma)}) \tag{B2}$$

for the junction occupancy $\tilde{\rho}^{(\sigma)}$ characterizing this plateau. In order to establish the density range corresponding to this plateau,

$$\bar{P}^{(\sigma)} = [\rho_-^{(\sigma)}, \rho_+^{(\sigma)}], \tag{B3}$$

some further thought is necessary.

We first consider the subsequent density range,

$$P^{(\sigma)} = [\rho_+^{(\sigma)}, \rho_*^{(\sigma)}], \tag{B4}$$

for which this particular loop has already reached a HD phase but no further loop has attained coexistence yet: this happens at the end of the corresponding density zone $\rho_*^{(\sigma)}$ (which also corresponds to the onset of the following plateau for the next bias: $\rho_*^{(\sigma_i)} = \rho_-^{(\sigma_{i+1})}$). In $P^{(\sigma)}$ the overall density can be written as

$$\begin{aligned} \rho &= \frac{1}{N}\sum_s \rho_s = \frac{1}{N}\left[\sum_{s\in\mathrm{HD}} \tilde{\rho} + \sum_{s\in\mathrm{LD}} \sigma_s\tilde{\rho}\right] \\ &= \frac{1}{N}\left[n(s{:}\sigma_s \geqslant \sigma) + \sum_{s:\sigma_s<\sigma} \sigma_s\right]\tilde{\rho} \quad (\rho \in P^{(\sigma)}), \end{aligned} \tag{B5}$$

where $n(s{:}\sigma_s \geqslant \sigma)$ is the count of segments with a bias σ_s at least as favorable as the given bias σ (recall that we have ordered the bias parameters, such that $\sigma_1 \geqslant \sigma_2 \geqslant \cdots \geqslant \sigma_N$). Therefore, the junction occupancy $\tilde{\rho}$ is related to the overall density ρ through

$$\tilde{\rho}^{(\sigma)} = \frac{N\,\rho}{n(s{:}\sigma_s \geqslant \sigma) \;+\; \sum_{s:\sigma_s<\sigma} \sigma_s} \qquad (\rho \in P^{(\sigma)}). \tag{B6}$$

The bounds $\rho_{\pm}^{(\sigma)}$ of the density range $\bar{P}^{(\sigma)}$ for which there is coexistence in the loop(s) with bias σ can now be determined from the intersection of the corresponding plateau value $\tilde{\rho}^{(\sigma)}$ [Eq. (B2)] with the adjacent linear zones [Eq. (B6)] immediately left and right. This establishes the plateau range as

$$\rho_{-}^{(\sigma)} = \frac{n(s{:}\sigma_s{>}\sigma) + \sum_{s:\sigma_s\leqslant\sigma} \sigma_s}{N\,(1+\sigma)}, \tag{B7}$$

$$\rho_{+}^{(\sigma)} = \frac{n(s{:}\sigma_s{\geqslant}\sigma) + \sum_{s:\sigma_s<\sigma} \sigma_s}{N\,(1+\sigma)}. \tag{B8}$$

The currents through the segments can now be deduced using the effective rates, i.e., more precisely, from $\beta_s = 1-\tilde{\rho}$ for HD segments and from $\alpha_s = \sigma_s\,\tilde{\rho}$ for those in LD. Therefore, the total current through the junction is

$$\tilde{J} = \sum_{s\in\mathrm{HD}} \tilde{\rho}(1-\tilde{\rho}) + \sum_{s\in\mathrm{LD}} \sigma_s\tilde{\rho}\,(1-\sigma_s\tilde{\rho}) \tag{B9}$$

$$= \sum_{s:\sigma_s\geqslant\sigma} \tilde{\rho}(1-\tilde{\rho}) + \sum_{s:\sigma_s<\sigma} \sigma_s\tilde{\rho}\,(1-\sigma_s\tilde{\rho}). \tag{B10}$$

This is the mean-field prediction used in Fig. 6. Note that it has been established assuming that no segments are in LD-HD coexistence, but it trivially also covers this case: the condition for coexistence on a segment being $\alpha_s = \beta_s$, i.e., $\sigma_s\tilde{\rho} = 1-\tilde{\rho}$, implies that it does not matter whether the corresponding segments are counted in the LD or the HD contributions.

This expression for the current also shows that the *first* current plateau is optimal, in the sense that all successive plateaus correspond to weaker currents. The optimal density region is therefore

$$\frac{1}{N(1+\sigma_1)} < \rho < \frac{n(s{:}\sigma_s{=}\sigma) + \sum_{s:\sigma_s<\sigma_1} \sigma_s}{N(1+\sigma_1)}. \tag{B11}$$

Finally, we point out in passing that the case of degenerate loops, i.e., several loops being fed with the same bias parameter, introduces no further subtleties when using this notation. It is handled by the above discussion, provided only that one remembers to account for all of those loops in the sums above and/or in the segment counts, such as $n(s{:}s{>}\sigma)$. The point at which the MC phase arises in the next loop(s), leading to saturation, naturally extends the notion of efficient and saturated pumping to a multiloop system with bias.

APPENDIX C: REFINED MEAN-FIELD ARGUMENTS

The mean-field analysis of TASEP segments employed most commonly is based on a homogeneous density throughout the segment. Both exact theories and simulations show that this is indeed the case, *except* for small boundary zones, where boundary layers in the density profiles allow us to match the currents as required.

As an example, consider a single segment in a LD phase, with entrance rate α and exit rate β. The mean-field prediction is a homogeneous density $\rho = \alpha$, which is consistent at the entry but can not hold at the exit: if the last site were at this density, the exit current would be $\rho\,\beta$, which would not generally match the entrance current $J = \alpha\,(1-\rho) = \alpha\,(1-\alpha)$. The solution to this apparent paradox lies in a boundary layer close to the exit, a very localized zone where the density profile varies continuously along the segment in order to ensure current conservation between neighboring sites:

$$\rho_i\,(1-\rho_{i+1}) = J = \rho_L\,\beta, \tag{C1}$$

where $i = 1 \ldots L$ is the number of the site along the segment. This is known to lead to density variations only in localized boundary layers [33], and the simplistic picture of a homogeneous density is therefore in fact valid.

Here, we use the above relation in order to deduce the density at the exit site ρ_L as

$$\rho_{\mathrm{exit}} = \rho_L = \frac{\alpha\,(1-\alpha)}{\beta}. \tag{C2}$$

In the N-fold loop, the effective entry and exit rates are given by the density $\tilde{\rho}$ at the junction site, as

$$\alpha = \nu\,\sigma\,\tilde{\rho} \qquad \text{and} \qquad \beta = 1-\tilde{\rho}. \tag{C3}$$

Using these rates in the boundary layer argument then leads to refined expressions for the density at the exit site:

$$\rho_{\mathrm{exit}}^{(s)} = \frac{2\sigma^{(s)}\rho(1-2\sigma^{(s)}\rho)}{1-\frac{2\rho}{\nu}} \qquad \text{(LD)}. \tag{C4}$$

For a HD phase the density at the entry site can be been obtained from equivalent arguments:

$$\rho_{\mathrm{entry}}^{(s)} = 1 - \frac{1-\rho}{\nu\sigma^{(s)}} \qquad \text{(HD)}. \tag{C5}$$

APPENDIX D: RECAPITULATING THE MEAN-FIELD RESULTS

Here, we summarize all mean-field results as we have established them for the various cases discussed in the main text, including several refined predictions (see above). The curves shown in Figs. 11 and 15 are based on these expressions. For ease of reference, we organize the results for each scenario in the form of a table (see Tables I and II).

All entries in these tables correctly reduce to those in Table I for neutral pumping and no bias ($\nu = 1$ and $\sigma_1 = \sigma_2 = 1/2$). Refined mean-field predictions incorporating the effect of boundary layers, as discussed in the main text, are given where appropriate. In those entries, the refined predictions appear first, followed by the nonrefined predictions.

TABLE I. Mean-field expressions, in absence of bias ($\sigma_i = 1/N$), in an N-fold loop. Refined mean-field results are indicated by an asterisk. Figure 11 exploits these results for a twofold loop ($N = 2$).

Phase	Density interval	J	ρ_{entry}	ρ_{exit}	$\tilde{\rho}$
Without pumping ($\nu = 1$)					
LD:LD	$0 < \rho < \frac{1}{N+1}$	$N\rho(1-\rho)$	ρ	$\frac{\rho(1-\rho)}{1-N\rho}$ (*)	$N\rho$
LD-HD:LD-HD	$\frac{1}{N+1} < \rho < \frac{N}{N+1}$	$\frac{N^2}{(N+1)^2}$	$\frac{1}{N+1}$	$\frac{N}{N+1}$	$\frac{N}{N+1}$
HD:HD	$\frac{N}{N+1} < \rho < 1$	$N\rho(1-\rho)$	$1 - N(1-\rho)$ (*)	ρ	ρ
With pumping ($\nu > 1$)					
LD:LD	$0 < \rho < \frac{1}{2}$	$N\rho(1-\rho)$	ρ	$\frac{\rho(1-\rho)}{1-\frac{N\rho}{\nu}}$ (*)	$\frac{N\rho}{\nu}$
MC:MC	$\rho = \frac{1}{2}$	$\frac{1}{2}$	$\in \left[\frac{1}{2}, \frac{2\nu/N+1}{2\nu/N}\right]$ (*)	$\in \left[\frac{\nu/N}{2(2\nu/N-1)}, \frac{1}{2}\right]$ (*)	$\in [\frac{1}{2\nu/N}, \frac{1}{2}]$
HD:HD	$\frac{1}{2} < \rho < 1$	$N\rho(1-\rho)$	$1 - \frac{1-\rho}{\nu/N}$ (*)	ρ	ρ

TABLE II. Mean-field expressions for a twofold loop with two distinct bias parameters ($\sigma_1 > \sigma_2$). Refined mean-field results are indicated by an asterisk.

Phase	Density interval	J	$\begin{Bmatrix}\rho_{\text{entry},1}\\ \rho_{\text{entry},2}\end{Bmatrix}$	$\begin{Bmatrix}\rho_{\text{exit},1}\\ \rho_{\text{exit},2}\end{Bmatrix}$	$\tilde{\rho}$
Weak pumping ($\nu < \frac{1}{\sigma_1} < \frac{1}{\sigma_2}$)					
LD:LD	$0 < \rho < \frac{\nu}{2(1+\nu\sigma_1)}$	$2\rho - (2\rho)^2\left(\sigma_1^2 + \sigma_2^2\right)$	$\begin{Bmatrix}2\sigma_1\rho\\ 2\sigma_2\rho\end{Bmatrix}$	$\begin{Bmatrix}\frac{2\sigma_1\rho(1-2\sigma_1\rho)}{1-\frac{2\rho}{\nu}}\ (*)\\ \frac{2\sigma_2\rho(1-2\sigma_2\rho)}{1-\frac{2\rho}{\nu}}\ (*)\end{Bmatrix}$	$\frac{2\rho}{\nu}$
LD-HD:LD	$\frac{1}{2}\frac{\nu}{1+\nu\sigma_1} < \rho < \frac{1}{2}\frac{1+\nu\sigma_2}{1+\nu\sigma_1}$	$\frac{\nu-\nu^2\sigma_2^2}{(1+\nu\sigma_1)^2}$	$\begin{Bmatrix}\frac{\nu\sigma_1}{1+\nu\sigma_1}\\ 2\sigma_2\rho\end{Bmatrix}$	$\begin{Bmatrix}\frac{1}{1+\nu\sigma_1}\ (*)\\ \frac{\sigma_2}{\sigma_1}\left(1-\frac{\nu\sigma_2}{1+\nu\sigma_1}\right)(*)\end{Bmatrix}$	$\frac{1}{1+\nu\sigma_1}$
HD:LD	$\frac{1}{2}\frac{1+\nu\sigma_2}{1+\nu\sigma_1} < \rho < \frac{1}{2}$	$2\,\rho - \frac{(2\rho)^2(1+\nu^2\sigma_2^2)}{(1+\nu\sigma_2)^2}$	$\begin{Bmatrix}\frac{2\rho}{1+\nu\sigma_2}\\ \frac{2\nu\sigma_2\rho}{1+\nu\sigma_2}\end{Bmatrix}$	$\begin{Bmatrix}\frac{2\rho}{1+\nu\sigma_2}\\ \frac{\nu\sigma_2\,2\rho}{1+\nu\sigma_2}\left(1-\frac{\nu\sigma_2\,2\rho}{1+\nu\sigma_2}\right)\\ \hline 1-\frac{2\rho}{1+\nu\sigma_2}\end{Bmatrix}(*)$	$\frac{2\rho}{1+\nu\sigma_2}$
HD:LD-HD	$\frac{1}{2} < \rho < \frac{1}{1+\nu\sigma_2}$	$\frac{2\nu\sigma_2}{(1+\nu\sigma_2)^2}$	$\begin{Bmatrix}\frac{1}{1+\nu\sigma_2}\\ \frac{\nu\sigma_2}{1+\nu\sigma_2}\end{Bmatrix}$	$\begin{Bmatrix}\frac{1}{1+\nu\sigma_2}\\ \frac{1}{1+\nu\sigma_2}\end{Bmatrix}$	$\frac{1}{1+\nu\sigma_2}$
HD:HD	$\frac{1}{1+\nu\sigma_2} < \rho < 1$	$2\rho(1-\rho)$	$\begin{Bmatrix}\rho\\ 1-\frac{1-\rho}{\nu\sigma_2}\end{Bmatrix}$	$\begin{Bmatrix}\rho\\ \rho\end{Bmatrix}$	ρ
Intermediate pumping ($\frac{1}{\sigma_1} < \nu < \frac{1}{\sigma_2}$)					
LD:LD	$0 < \rho < \frac{1}{2}\frac{1}{2\sigma_1}$	$2\rho - (2\rho)^2(\sigma_1^2 + \sigma_2^2)$	$\begin{Bmatrix}2\sigma_1\rho\\ 2\sigma_2\rho\end{Bmatrix}$	$\begin{Bmatrix}\frac{2\sigma_1\rho(1-2\sigma_1\rho)}{1-\frac{2\rho}{\nu}}\ (*)\\ \frac{2\sigma_2\rho(1-2\sigma_2\rho)}{1-\frac{2\rho}{\nu}}\ (*)\end{Bmatrix}$	$\frac{2\rho}{\nu}$
MC:LD	$\frac{1}{2}\frac{1}{2\sigma_1} < \rho < \frac{1}{2}\frac{1+\nu\sigma_2}{2}$	$2\,(2\rho) - (2\rho)^2 - \frac{1}{2}$	$\begin{Bmatrix}1-\frac{\sigma_2}{4\sigma_1(2\rho-\frac{1}{2})}\ (*)\\ 2\rho - \frac{1}{2}\end{Bmatrix}$	$\begin{Bmatrix}\frac{\nu\sigma_2^2}{4(\nu\sigma_2-2\rho+\frac{1}{2})}\ (*)\\ \frac{(2\rho-\frac{1}{2})(\frac{3}{2}-2\rho)}{1-\frac{2\rho-\frac{1}{2}}{\nu\sigma_2}}\end{Bmatrix}$	$\frac{2\rho-\frac{1}{2}}{\nu\sigma_2}$
HD:LD	$\frac{1}{2}\frac{1+\nu\sigma_2}{2} < \rho < \frac{1}{2}$	$2\rho - \frac{(2\rho)^2(1+\nu^2\sigma_2^2)}{(1+\nu\sigma_2)^2}$	$\begin{Bmatrix}1-\frac{1-\frac{2\rho}{1+\nu\sigma_2}}{\nu\sigma_1}\ (*)\\ \frac{\nu 2\sigma_2\rho}{1+\nu\sigma_2}\end{Bmatrix}$	$\begin{Bmatrix}\frac{2\rho}{1+\nu\sigma_2}\\ \frac{\nu\sigma_2\,2\rho}{1+\nu\sigma_2}\left(1-\frac{\nu\sigma_2\,2\rho}{1+\nu\sigma_2}\right)\\ \hline 1-\frac{2\rho}{1+\nu\sigma_2}\end{Bmatrix}(*)$	$\frac{2\rho}{1+\nu\sigma_2}$
HD:LD-HD	$\frac{1}{2} < \rho < \frac{1}{1+\nu\sigma_2}$	$\frac{2\nu\sigma_2}{(1+\nu\sigma_2)^2}$	$\begin{Bmatrix}1-\frac{\sigma_2}{\sigma_1(1+\nu\sigma_2)}\ (*)\\ \frac{\nu\sigma_2}{1+\nu\sigma_2}\end{Bmatrix}$	$\begin{Bmatrix}\frac{1}{1+\nu\sigma_2}\\ \frac{1}{1+\nu\sigma_2}\end{Bmatrix}$	$\frac{1}{1+\nu\sigma_2}$
HD:HD	$\frac{1}{1+\nu\sigma_2} < \rho < 1$	$2\rho(1-\rho)$	$\begin{Bmatrix}1-\frac{1-\rho}{\nu\sigma_1}\ (*)\\ 1-\frac{1-\rho}{\nu\sigma_2}\ (*)\end{Bmatrix}$	$\begin{Bmatrix}\rho\\ \rho\end{Bmatrix}$	ρ
Strong pumping ($\frac{1}{\sigma_1} < \frac{1}{\sigma_2} < \nu$)					
LD:LD	$0 < \rho < \frac{1}{2}\frac{1}{2\sigma_1}$	$2\rho - (2\rho)^2\left(\sigma_1^1 + \sigma_2^2\right)$	$\begin{Bmatrix}2\sigma_1\rho\\ 2\sigma_2\rho\end{Bmatrix}$	$\begin{Bmatrix}\frac{2\sigma_1\rho(1-2\sigma_1\rho)}{1-\frac{2\rho}{\nu}}\ (*)\\ 2\sigma_2\rho\end{Bmatrix}$	$\frac{2\rho}{\nu}$
MC:LD	$\frac{1}{2}\frac{1}{2\sigma_1} < \rho < \frac{1}{2}$	$2\,(2\rho) - (2\rho)^2 - \frac{1}{2}$	$\begin{Bmatrix}1-\frac{\sigma_2}{4\sigma_1(2\rho-\frac{1}{2})}\ (*)\\ 2\rho - \frac{1}{2}\end{Bmatrix}$	$\begin{Bmatrix}\frac{\nu\sigma_2}{4(\nu\sigma_2-2\rho+\frac{1}{2})}\ (*)\\ 2\rho - \frac{1}{2}\end{Bmatrix}$	$\frac{2\rho-\frac{1}{2}}{\nu\sigma_2}$
MC:MC	$\rho = \frac{1}{2}$	$\frac{1}{2}$	$\begin{Bmatrix}\in [\frac{2\sigma_1-\sigma_2}{2\sigma_1}, \frac{1+2(\nu\sigma_1-1)}{2\nu\sigma_1}]\\ \in [\frac{1}{2}, \frac{1+2(\nu\sigma_2-1)}{2\nu\sigma_2}]\end{Bmatrix}$	$\begin{Bmatrix}\in [\frac{\nu\sigma_2}{4(\nu\sigma_2-\frac{1}{2})}, \frac{1}{2}]\\ \frac{1}{2}\end{Bmatrix}$	$\in \left[\frac{1}{2\nu\sigma_2}, \frac{1}{2}\right]$
HD:HD	$\frac{1}{2} < \rho < 1$	$2\rho(1-\rho)$	$\begin{Bmatrix}1-\frac{1-\rho}{\nu\sigma_1}\ (*)\\ 1-\frac{1-\rho}{\nu\sigma_2}\ (*)\end{Bmatrix}$	$\begin{Bmatrix}\rho\\ \rho\end{Bmatrix}$	ρ

[1] C. T. MacDonald, J. H. Gibbs, and A. C. Pipkin, Biopolymers **6**, 1 (1968).
[2] Q.-H. Wei, C. Bechinger, and P. Leiderer, Science **287**, 625 (2000).
[3] K. Heckmann, B. Lindemann, and J. Schnakenberg, Biophysical Journal **12**, 683 (1972).
[4] T. Reichenbach, E. Frey, and T. Franosch, New J. Phys. **9**, 159 (2007).
[5] A. Roux, G. Capello, J. Cartaud, J. Prost, B. Goud, and P. Bassereau, Proc. Natl. Acad. Sci. USA **99**, 5394 (2002).
[6] G. Koster, M. VanDuijn, B. Hofs, and M. Dogterom, Proc. Natl. Acad. Sci. USA **100**, 15583 (2003).
[7] C. Leduc, O. Campas, K. B. Zeldovich, A. Roux, P. Jolimaitre, L. Bourel-Bonnet, B. Goud, J.-F. Joanny, P. Bassereau, and J. Prost, Proc. Natl. Acad. Sci. USA **101**, 17096 (2004).
[8] K. Nagel, Phys. Rev. E **53**, 4655 (1996).
[9] C. Appert-Rolland, J. Cividini, and H. J. Hilhorst, J. Stat. Mech. (2011) P10014.
[10] B. Derrida, E. Domany, and D. Mukamel, J. Stat. Phys. **69**, 667 (1992).
[11] G. M. Schütz, J. Stat. Phys. **88**, 427 (1997).
[12] B. Derrida and M. R. Evans, in *Non-equilibrium Statistical Mechanics in One Dimension*, edited by V. Privman (Cambridge University Press, Cambridge, UK, 1997), pp. 277–304.
[13] A. B. Kolomeisky, G. M. Schutz, E. B. Kolomeisky, and J. P. Straley, J. Phys. A: Math. Gen. **31**, 6911 (1998).
[14] J. Snider, F. Lin, N. Zahedi, V. Rodionov, C. C. Yu, and S. P. Gross, Proc. Natl. Acad. Sci. USA **101**, 13204 (2004)
[15] J. L. Ross, H. Shuman, E. L. F. Holzbaur, and Y. E. Goldman, Biophys. J. **94**, 3115 (2008).
[16] S. Bálint, I. Verdeny Vilanova, A. Sandoval Alvarez, and M. Lakadamyali, Proc. Natl. Acad. Sci. USA **110**, 3375 (2013).
[17] B. Alberts, D. Bray, J. Lewis, M. Raff, K. Roberts, and J. D. Watson, *Molecular biology of the cell* (Garland, New York, 1994).
[18] Cécile C. Leduc, Kathrin K. Padberg-Gehle, Vladimír V. Varga, Dirk D. Helbing, Stefan S. Diez, and Jonathon J. Howard, Proc. Natl. Acad. Sci. USA **109**, 6100 (2012).
[19] P. Greulich and L. Santen, Eur. Phys. J. E **32**, 191 (2010).
[20] I. Neri, N. Kern, and A. Parmeggiani, Phys. Rev. Lett. **107**, 068702 (2011).
[21] I. Neri, N. Kern, and A. Parmeggiani, Phys. Rev. Lett. **110**, 098102 (2013).
[22] I. Neri, N. Kern, and A. Parmeggiani, New J. Phys. **15**, 085005 (2013).
[23] N. Crampé and A. Trombettoni, Nucl. Phys. B **871**, 526 (2013).
[24] B. Embley, A. Parmeggiani, and N. Kern, Phys. Rev. E **80**, 041128 (2009).
[25] B. Derrida, J. L. Lebowitz, and E. R. Speer, J. Stat. Phys. **89**, 135 (1997).
[26] R. A. Blythe and M. R. Evans, J. Phys. A: Math. Theor. **40**, R333 (2007).
[27] A. Lazarescu and K. Mallick, J. Phys. A: Math. Theor. **44**, 315001 (2011).
[28] J. Brankov, N. Pesheva, and N. Bunzarova, Phys. Rev.E **69**, 066128 (2004).
[29] E. Pronina and A. B. Kolomeisky, J. Stat. Mech.: Theor. Exp: (2005) P07010.
[30] B. Embley, A. Parmeggiani, and N. Kern, J. Phys.: Condens. Matter **20**, 295213 (2008).
[31] Simulations consist in randomly picking particles and moving them whenever the next site is free. When a particle on a junction site is picked, one of the outgoing segments is chosen at random. "Bias" (see Sec. IV) is implemented by choosing the out-segments nonuniformly, according to their bias parameters. "Pumping" (see Sec. V) corresponds to picking particles on the junction site more often, according to the pumping rate.
[32] S. Rock, Curr. Biol. **22**, R606 (2012).
[33] G. Schutz and E. Domany, J. Stat. Phys. **72**, 277 (1993).